Research Article

Thanh-Nhut Pham, Quoc Tien Le, and Quang Thang Do*

Experimental and numerical investigations of multi-layered ship engine room bulkhead insulation thermal performance under fire conditions

Abstract: The thermal insulation layer of the ship's engine room bulkhead is typically constructed from multiple layers of mineral wool. This layer is designed to keep the temperature on the surface of the bulkhead below 140°C in case of a fire. However, measuring the inner and external temperatures of each wall panel bulkhead type during a fire can be difficult. To address this issue, this study was conducted to evaluate the multilayer heat transfer capability of the bulkhead insulation in the event of an engine room fire. The study used heat transfer theory, experimental models, and numerical analysis to assess nine bulkhead insulation specimens. These specimens were fabricated from three original specimens and included a 10–30 mm air layer (W-75, W-50, and W-25). The results showed that all improved specimens had better thermal insulation than the originals. Among them, the improved specimens derived from the W-25 specimen exhibited the most significant temperature reduction compared to those derived from the W-75 and W-50 specimens. The results demonstrated a slight difference between the three methodologies, indicating a high level of reliability in the research findings.

Keywords: heat transfer, insulation, engine room wall, fire protection, multi-layer structure

1 Introduction

Ships, especially oil tankers, have several areas that require thermal insulation and fire protection, and the engine room is one such area. In a steel-hulled cargo ship's engine room, you can find a variety of insulated walls, such as bulkheads, fuel tank walls, and ceilings as shown in Figure 1. The structure of thermal insulation walls usually consists of wall panels, insulation layers, and surface materials. The typical structure of insulated and fire-resistant engine room walls is depicted in Figure 2 [1].

Various materials are used to meet thermal insulation and fire protection standards for different types of walls. Typically, individual insulation layers are installed in walls, floors, and ceilings to achieve this purpose, as shown in Figure 3. However, in certain areas with high combustion temperatures or excessive noise levels, it may be necessary to use two to four layers of insulation (Figure 4) [2].

Extensive global research efforts have been devoted to investigating the potential of ceramic materials, basalt fibers, and mineral wool for thermal insulation and fire protection. These materials have been subjected to rigorous analysis, including extensive examination of their physical and chemical properties and manufacturing techniques. As a result, they have become widely adopted within a range of industries, including construction, shipbuilding, automotive, and aerospace. Significantly, mineral wool has emerged as the most preferred thermal insulation and fire protection form in steel-hulled cargo ships [3].

Mineral wool is an insulation material made by melting Basalt ore and Dolomite rock at high temperatures (*i.e.*, 1,600°C). The molten material is then spun into small fibers mixed with specialized chemicals. Mineral wool is available in various forms, including rolls, pipes, and panels, making it easy to install in construction projects. In addition, it is cost-effective and convenient to transport.

* **Corresponding author: Quang Thang Do,** Department of Naval Architecture and Ocean Engineering, Nha Trang University, Nha Trang 650000, Vietnam, e-mail: thangdq@ntu.edu.vn
Thanh-Nhut Pham: Department of Naval Architecture and Ocean Engineering, Nha Trang University, Nha Trang 650000, Vietnam
Quoc Tien Le: Hyundai-Vietnam Shipbuilding Co., LTD, Nha Trang 650000, Vietnam
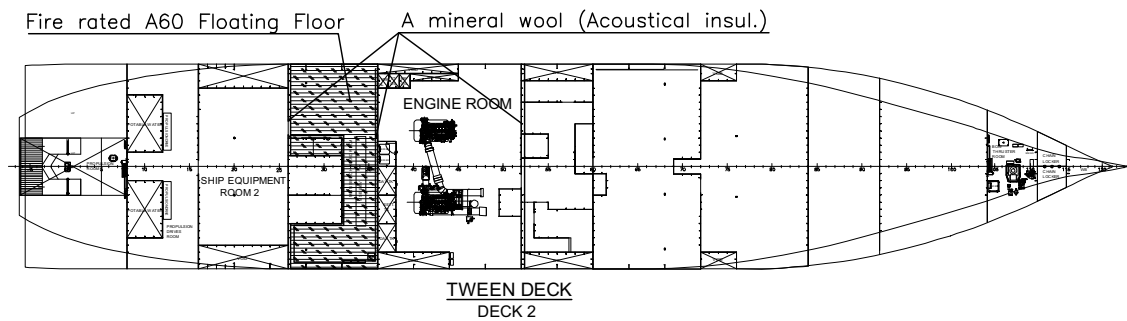
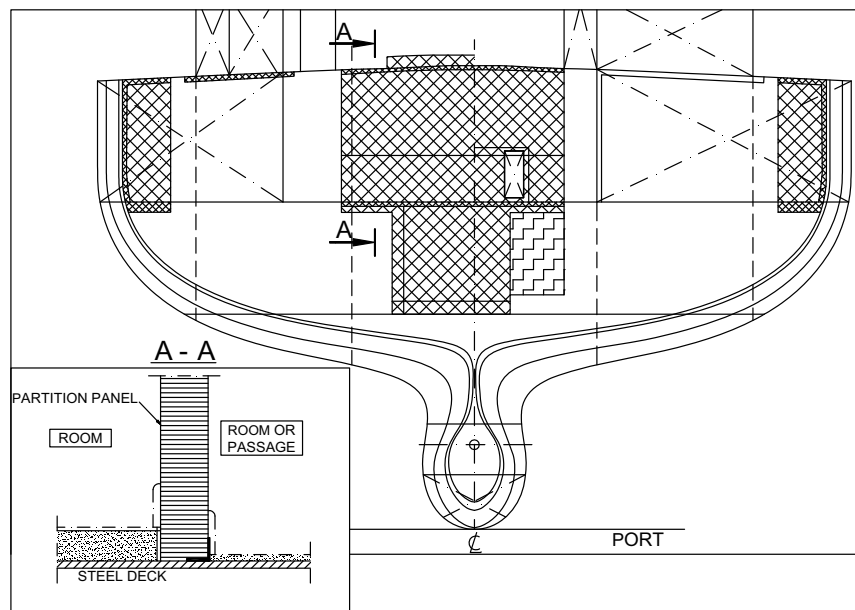**Figure 1:** Locations needing ship thermal insulating walls.

Figure 2: Engine room bulkhead with a fire-insulating structure [1].

Mineral wool is a term that encompasses mineral fibers with a woolly consistency, which are typically derived from molten glass, rock, or slag. Glass wool, which is produced from molten glass, and rock wool, which is derived from naturally occurring igneous rock, are two types of mineral wool. Slag wool, on the other hand, is produced from furnace slag that has been melted. Keith [4] has defined mineral wool as a generic term. He has noted that rock wool products can be used up to 1,100°C, although it is recommended that they be operated at a maximum temperature of 850°C. This is a testament to the unique capabilities of rock wool products. In conclusion, mineral wool is a versatile material that can be used in a variety of applications. It is important to understand the differences between the various types of mineral wool to select the appropriate product for a given use case.

Rock wool and slag wool have excellent fire resistance properties due to their physical and chemical characteristics. The fibers in these materials are noncombustible and have melting temperatures above 2,000°F, which provides effective sound control, fire protection, and attenuation capabilities. Furthermore, mineral wool is ideal for insulating chimney areas because it cannot support combustion [5].

Numerous studies have been conducted on heat transfer issues and thermal insulation materials. Mahdi *et al.* [6] studied the use of atmospheric plasma spraying and yttria-stabilized zirconia nanostructured coatings on the bond layer of NiCrAlY-coated engine cylinder heads, pistons, and valve substrates. They utilized thermal barrier coatings to enhance engine performance during the construction of combustion chamber parts for internal combustion engines. Their research showed a significant improvement in binding
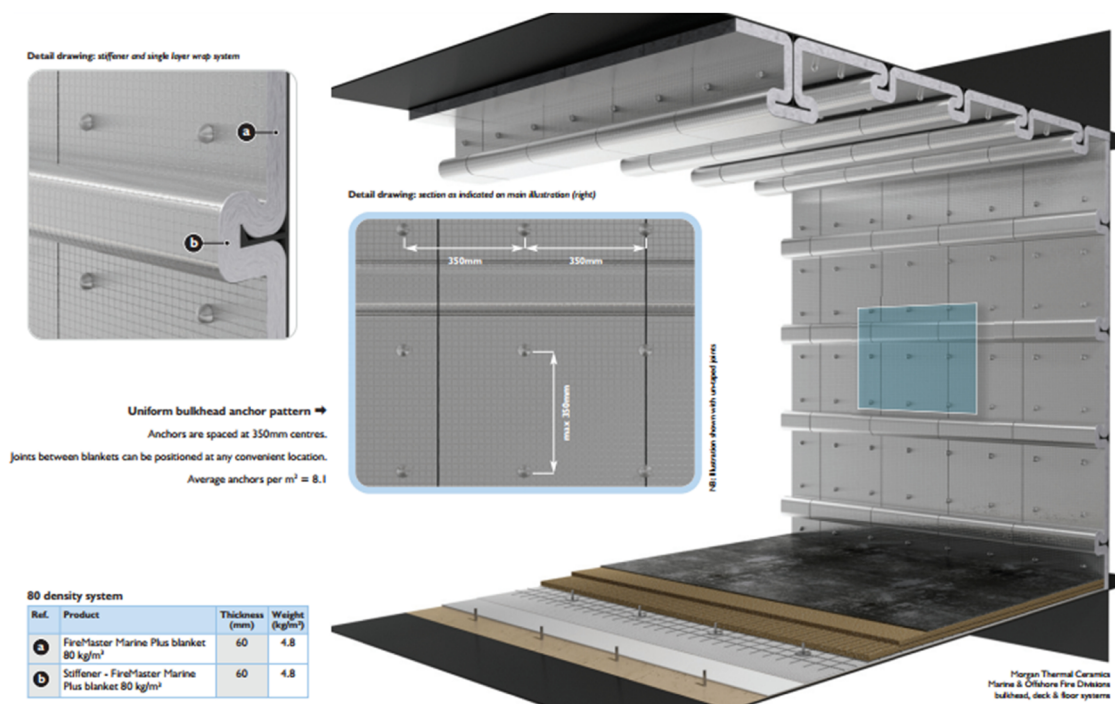
Figure 3: Arrangement of a single layer of thermal insulation for the walls and ceiling structures [2].

strength and thermal insulation capacity. Dimitri *et al.* [7] conducted a study on the bond performance of fibreglass reinforced plastic laminates attached to concrete surfaces exposed to heat fluctuations. Their study analyzed the impact of adhesive geometrical features and temperature-dependent mechanical properties on bond behavior and failure scenarios. In addition, other research studies have been carried out on sandwich constructions, focusing on mechanical and thermal properties [8–10].

Regarding the heat transfer calculation methods for ship walls, there are several references on the theoretical foundations of steady-state and unsteady-state heat transfer and multilayer partitions [5,11–13]. Furthermore, some studies on insulation and fire protection for seafaring vessels and offshore structures have also been published, such as those by Yizhou *et al.* [14] and Pierre and David [15]. Specifically, Yunus and Afshin [16] provide a highly detailed reference on heat and mass transfer fundamentals and applications, including a study on steady heat conduction in-plane walls. They used the steady heat conduction problem in multilayer plane walls as a theoretical foundation to calculate the thermal insulation for the ship engine room bulkhead.

The engine room of a ship requires strict insulation and fire protection measures. According to regulations, if there is a gas discharge fire at 950°C for 60 min, the external surface of the bulkhead must not exceed 140°C. However, accurately determining the internal and external

temperatures for various bulkhead types becomes challenging in a fire. Therefore, this research aims to assess the heat transfer capabilities across the multilayer structure of the bulkhead when a fire breaks out in the engine room. The results obtained from this study will help to evaluate the bulkhead's effectiveness in insulation and fire protection. An experimental approach is being used in this study, utilizing bulkhead models for analysis.

2 Introduction to target structures

Many ships incorporate bulkheads, fire-resistant walls, floors, and ceilings into their design. This study specifically examines the thermal insulation (fire resistance) capabilities of the wall structure on a 50,000 deadweight tonnage (DWT) oil tanker (bulkhead numbers 10 and 39). At bulkhead No. 10, two different structures are present: one with a 75 mm thick insulation layer, called W-75 (Figure 5b), and the other with a 50 mm thick insulation layer, labeled W-50 (Figure 5c). Bulkhead number 39 has a 25 mm thick insulation layer, known as W-25 (Figure 5d). All three types of walls secure the insulation layer to the bulkhead's wall panel using evenly spaced fasteners at 300 mm intervals (Figure 5a). Accordingly, this study concentrates on a real wall panel at a watertight bulkhead with a 300×300 (mm^2) area, as depicted in Figure 6.

(a)

(b)

(c)
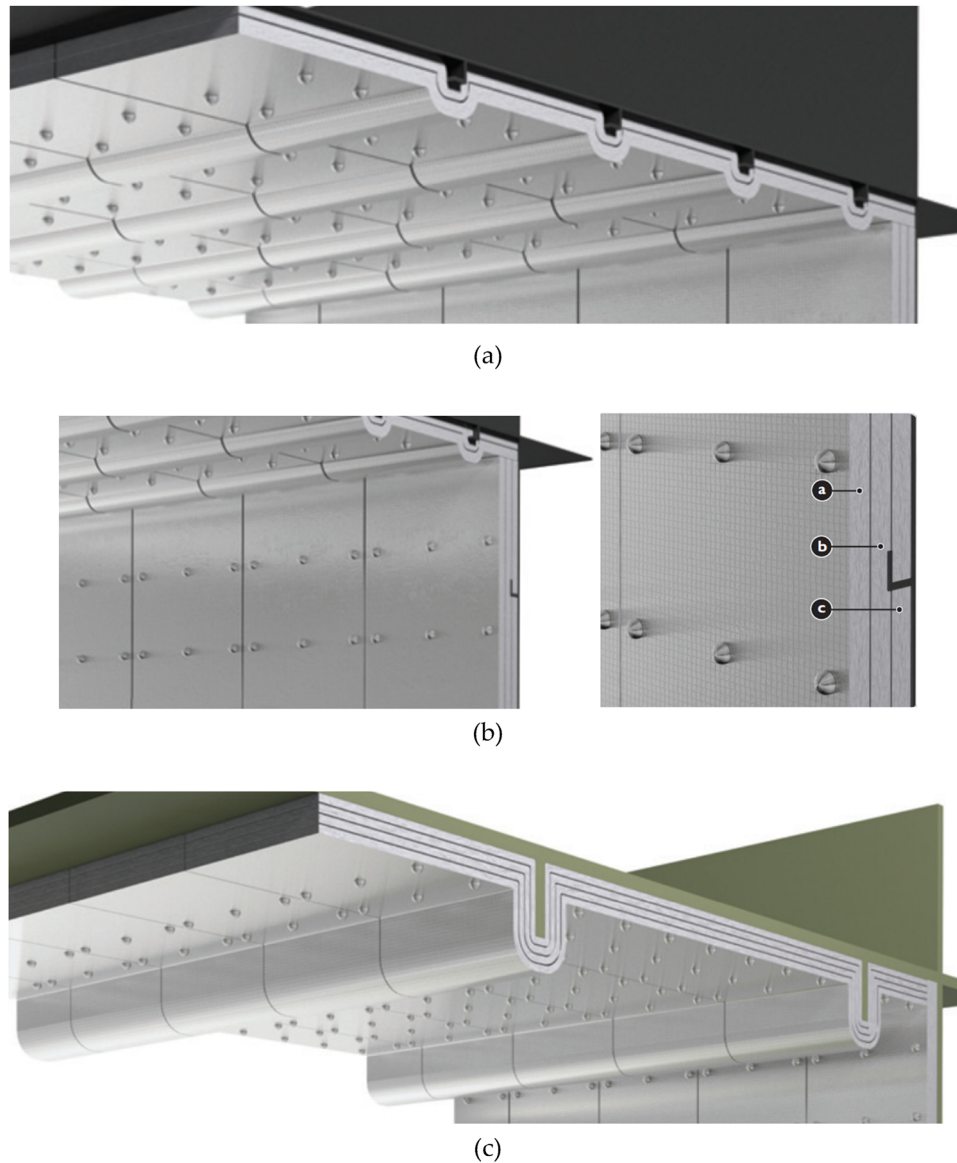
Figure 4: Types of structures arranged with multiple layers of thermal insulation: (a) two-layer fire insulation structures, (b) third-layer fire insulation structures, and (c) four-layer fire insulation structures.

Several novel structural wall models have been proposed based on research on the ship's actual structure. These wall structures have been further evaluated to assess their thermal effectiveness. As per standard recommendations [17], the glass woven roving layer (for W-75 types) or the cover layer (for W-50 and W-25 types) is directly exposed to flames in the event of a fire. The flames are sustained for a specific period, contingent on the type of mineral wool used, to attain a minimum temperature of 950°C. This temperature is then transferred through the wall structure's layers to the sheet's outer surface. It is imperative that the temperature on the outer surface of the sheet after a specific period, specific to the type of mineral wool used, should not exceed 140°C (averaged over the entire area) and 180°C (at any point on the surface), as detailed in Figure 6.

3 Method, materials, specimens, and testing equipment

To assess the thermal insulation capacity of the thermal insulation wall configurations discussed in Section 2, this research utilizes a combination of theoretical calculations and experimental testing on specimens.
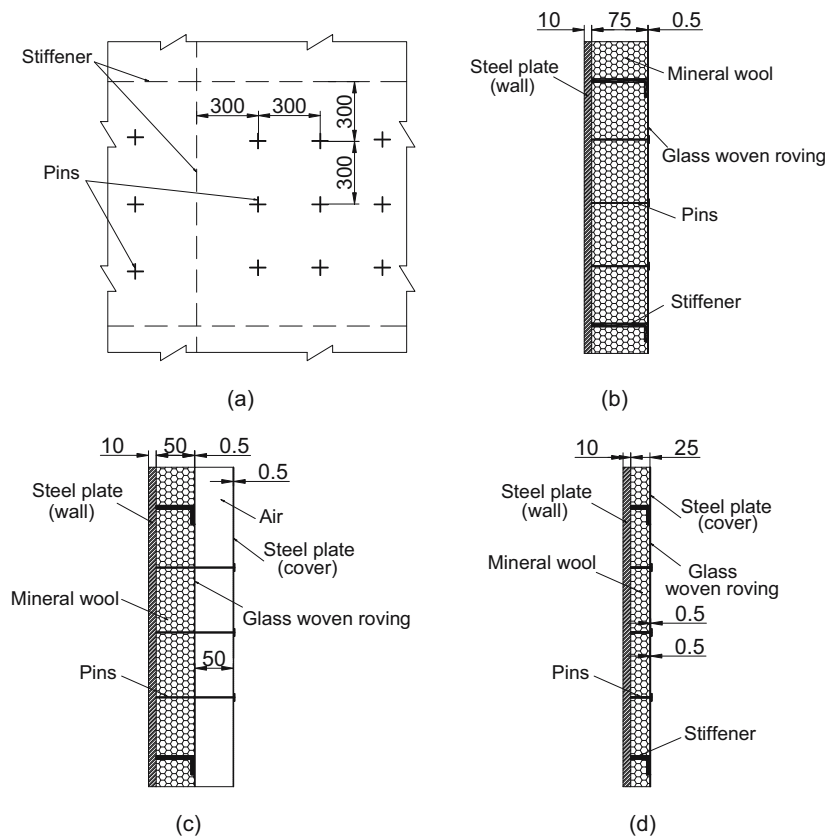
Figure 5: Three typical fire insulations: (a) arrangement of pinning distance at every 300 mm, (b) fire insulation with a thick of 75 mm (W-75), (c) fire insulation with a thick of 50 mm (W-50), and (d) fire insulation with a thick of 25 mm (W-25).
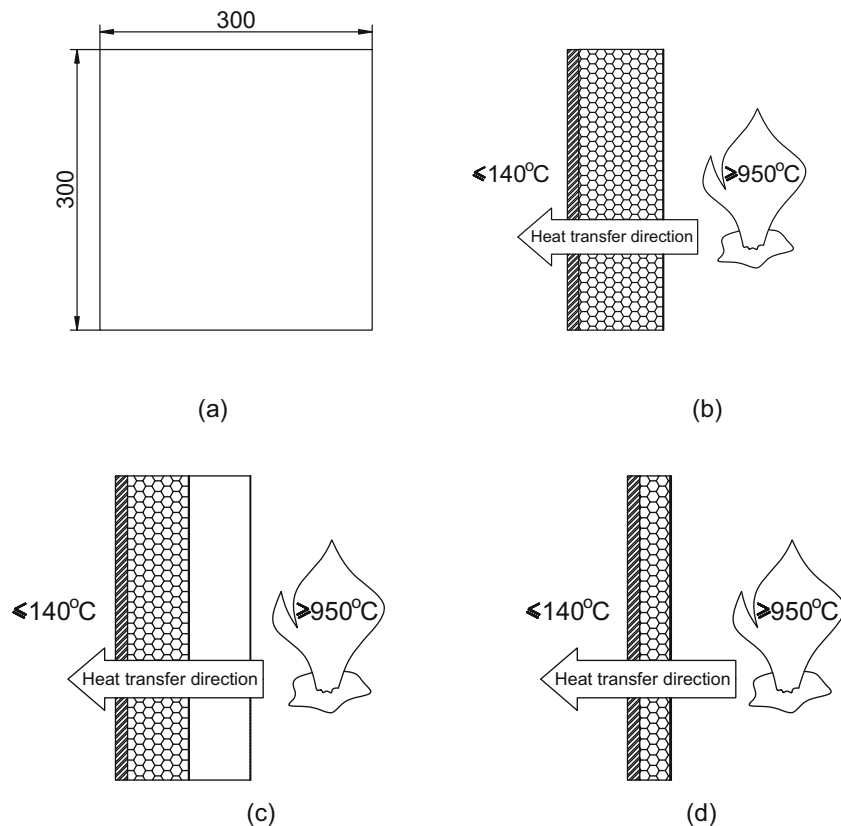
Figure 6: Specimens applied in this study: (a) dimension of specimen, (b) specimen W-75, (c) specimen W-50, and (d) specimen W-25.

3.1 Theoretical calculation

The present study calculates thermal insulation wall models for a 50,000 DWT steel-hulled oil tanker. The theory of steady heat conduction in multilayer plane walls [16] has been utilized for this purpose. The proposed method involves the analysis of the heat transfer mechanism through the walls of the oil tanker, taking into account the thermal resistance of each layer. The model has been developed to optimize the insulation properties of the wall while also ensuring that the vessel's structural integrity is maintained. This approach is expected to provide valuable insights into the design of thermal insulation systems for similar marine vessels. The heat transfer model through a single-layer flat wall is described in Figure 7. The model of heat transfer through a two-layer flat wall is presented in Figure 8.

• Heat conduction through a plane wall $\dot{Q}$(W):

$$\dot{Q} = \frac{T_{\infty 1} - T_{\infty 2}}{R_{\text{conv},1} + R_{\text{wall}} + R_{\text{conv},2}} \text{ (W)}, \tag{1}$$

where $T_{\infty 1}$ refers to the temperature in the combustion zone, which is essentially the temperature away from the
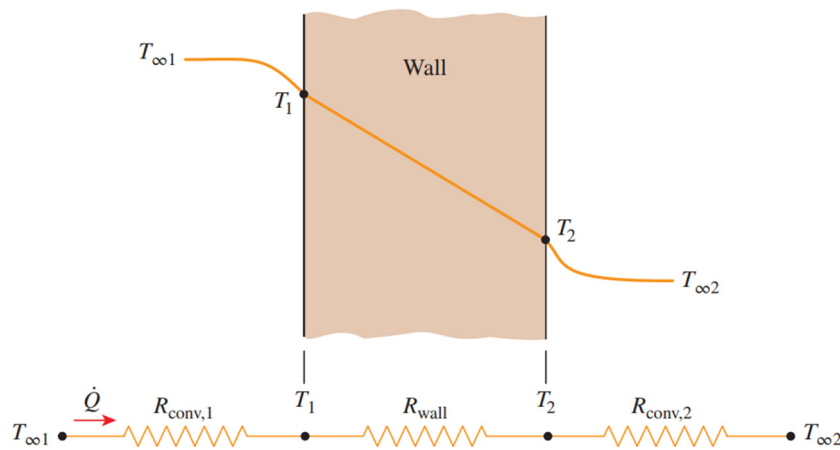
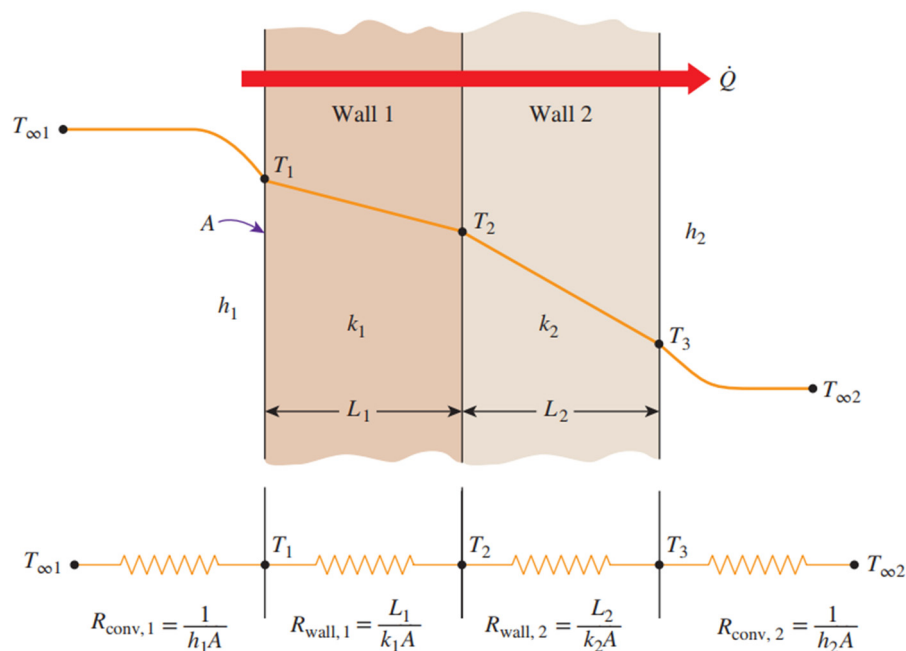**Figure 7:** Model of heat transfer through a single-layer flat wall.

Figure 8: Model of heat transfer through a two-layer flat wall.

wall surface. This temperature is commonly known as the hot side temperature and is measured in °K. $T_{\infty 2}$ represents the temperature in the noncombustion zone, specifically the temperature away from the wall surface. This temperature is commonly referred to as the cold side temperature and is measured in °K. $R_{conv,1}$ and $R_{conv,2}$ represent the thermal resistance at the hot and cold convective surfaces, respectively, measured in W/K. R_{wall} is thermal resistance of wall, W/K.

- Total of thermal resistance:

$$R_{total} = R_{conv,1} + R_{wall} + R_{conv,2} = \frac{1}{h_1 A} + \frac{1}{kA} + \frac{1}{h_2 A}, \quad (2)$$

where h_1 and h_2 are convection heat transfer coefficients of hot side and cold side (unit: W/m² K); k represents thermal conductivity (unit: W/m K); and A is the area of wall (unit: m²).

The determination of the convection heat transfer coefficient (h_i) for both the hot side (h_1) and the cold side (h_2) is crucial in many industrial and scientific applications. Several methods can be employed to obtain this coefficient, depending on the specific context of the process under investigation. Once determined, h_i can be used to calculate heat transfer rates and to optimize the design of heat exchangers and other thermal systems. In this study, the hot side (h_1) and cold side (h_2) can be determined by following the method proposed by Böckh and Thomas [11]:

$$h_i = Nu_i \frac{\lambda_i}{l}, \quad (3)$$

where λ_i is thermal conductivity of air (λ_1 for the hot side and λ_2 for the cold side), l – high of wall (m), and Nu is the Nußelt number (Nu_1 for hot side and Nu_2 for cold side).

$$Nu_i = \{0.825 + 0.387 Ra_i f_i(Pr)\}^2, \quad (4)$$

$$\text{For hot side : } Ra_1 = \frac{gH^3(T_{\infty 1} - T_1')}{T_{\infty 1} \nu_1^2} Pr_1, \quad (5)$$

$$\text{For cold side : } Ra_2 = \frac{gH^3(T_2' - T_{\infty 2})}{T_{\infty 2} \nu_2^2} Pr_2, \quad (6)$$

$$f_i(Pr) = (1 + 0.671 Pr_i^{-9/16})^{-8/27}, \quad (7)$$

where Ra is the Rayleigh number, Pr is the Prandtl number, T_1' is the temperature of air at hot side (°K), and T_2' is the temperature of air at cold side (°K).

- Heat conduction through a plane wall $\dot{Q}(W)$:

$$\dot{Q} = \frac{T_{\infty 1} - T_{\infty 2}}{R_{total}}, \quad (8)$$

where

$$R_{total} = R_{conv,1} + R_{wall,1} + R_{wall,2} + R_{conv,2}$$
$$= \frac{1}{h_1 A} + \frac{L_1}{k_1 A} + \frac{L_2}{k_2 A} + \frac{1}{h_2 A}. \quad (9)$$

- The thermal resistance of a flat wall with n layers may be calculated as follows:

$$R_{total} = R_{conv,1} + R_{wall,1} + R_{wall,2} + \cdots + R_{wall,n}$$
$$+ R_{conv,2} \quad (10)$$
$$= \frac{1}{h_1 A} + \frac{L_1}{k_1 A} + \frac{L_2}{k_2 A} + \cdots + \frac{L_n}{k_n A} + \frac{1}{h_2 A}.$$

The surface temperature of each wall layer T_i (where $i = 1, 2,..., n+1$) can be determined using the following formulas (11)–(14):

$$\dot{Q} = \frac{T_{\infty 1} - T_1}{R_{conv,1}}, \quad (11)$$

$$\dot{Q} = \frac{T_{\infty 1} - T_2}{R_{conv,1} + R_{wall,1}}, \quad (12)$$

$$\dot{Q} = \frac{T_{\infty 1} - T_3}{R_{conv,1} + R_{wall,1} + R_{wall,2}}, \quad (13)$$

$$\dot{Q} = \frac{T_{n+1} - T_{\infty 2}}{R_{conv,2}}. \quad (14)$$

3.2 Experiment

This study utilizes a testing method on specimens that closely resemble actual ship wall models measuring 300 × 300 mm. The specimens correspond to three types of flat walls found on a 50,000 DWT oil tanker, with designations W-75, W-50, and W-25. Each specimen has specific details, with the W-75 specimen consisting of three layers: wall panel (AH32 – 10 mm), mineral wool (A60 – 75 mm), and cloth (glass woven roving – 0.5 mm), as illustrated in Figure 9.
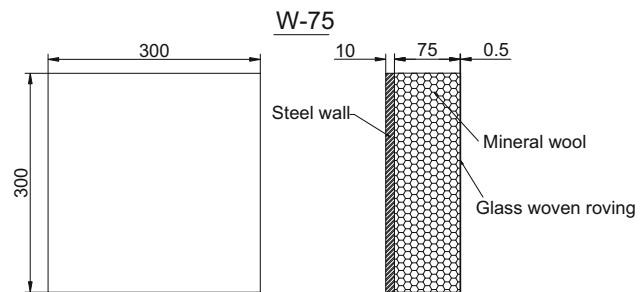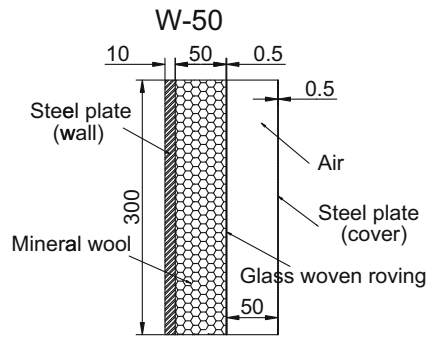

Figure 9: Specimens W-75.
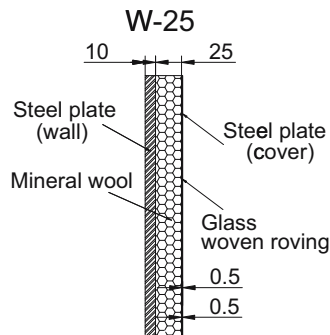
W-50

Figure 10: Specimen W-50.

W-25

Figure 11: Specimen W-25.

This study represents a significant advancement in ship-building, paving the way for safer and more efficient practices, which will contribute to the overall improvement of the industry.

The W-50 and W-25 specimens are each made up of four layers: a wall plate (AH32 – 10 mm), mineral wool (A60 – 50 mm for W-50 and 25 mm for W-25), a glass woven roving cloth (0.5 mm), and a cladding plate (galvanized steel 0.5T – 0.5 mm). The W-50 specimen is shown in Figure 10, while the W-25 specimen is shown in Figure 11. Each layer is described in detail in Figure 12.

The experiment involved heating the specimens by placing them in direct contact with a glass woven roving layer or a cover steel plate. The temperature was raised to 950°C and maintained for 60 min. To monitor the temperature, measurements were taken at three points on the surface of the wall steel plate every 5 min during the heating process. Each point was measured three times, and the final temperature recorded was the average of the three measurements taken at the three designated points, as presented in Figure 13.

The specimens were heated using the Nabertherm-MSH1 furnace (Germany) with the specifications provided in Table 1. The temperature was measured using the
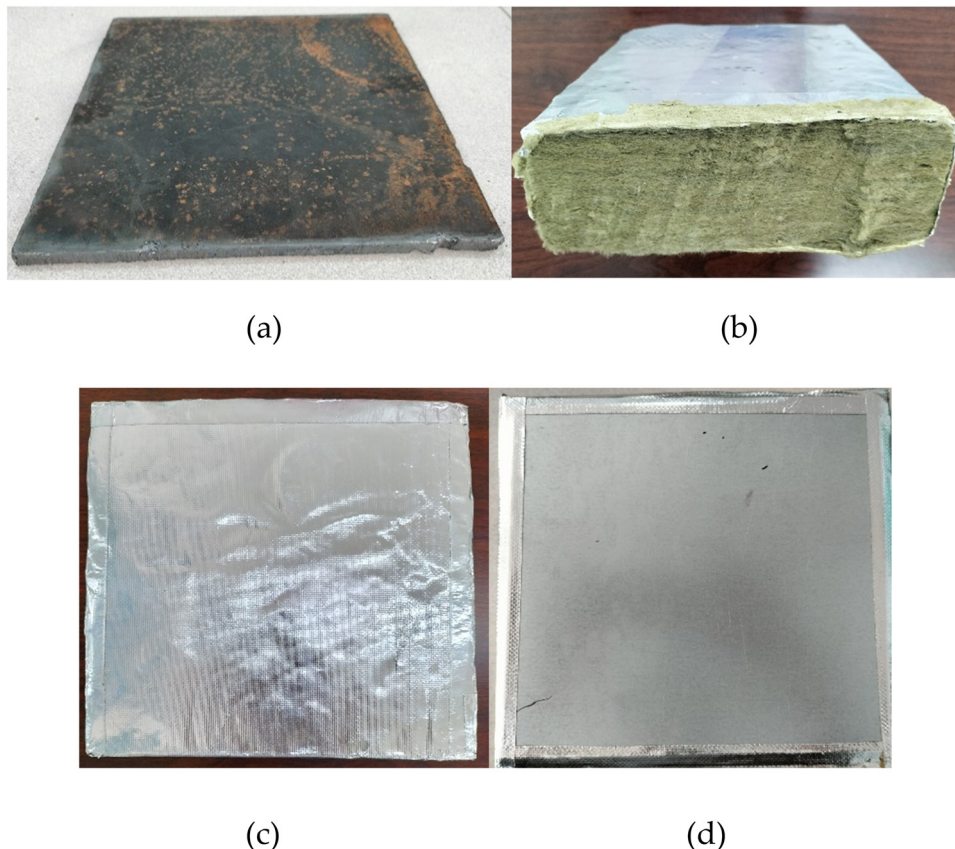

(a) (b)

(c) (d)

Figure 12: Material properties: (a) steel plate (wall), (b) Mineral wool, (c) Glass woven roving, (d) steel plate (cover).
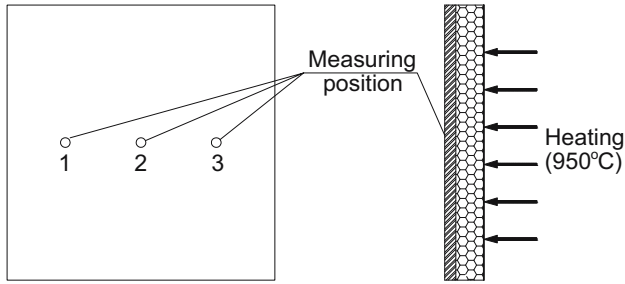
Figure 13: Heating and measurement locations on the specimen.

Table 1: Specifications of the Nabertherm-MSH1 furnace

Specification	Value	Unit
Applied temperature	30–3,000	°C
Maximum temperature	4,200	°C
Voltage	230	V
Power	3	kW

Table 2: Specifications of the Fluke-561 laser thermal gun

Specification	Value	Unit
Temperature measurement range	−40 to 550	°C
Tolerance	±0.1	°C
Voltage	12	V

Fluke-561 laser infrared thermometer (China) with the specifications provided in Table 2.

3.3 Material properties

The thermal insulation structure comprises three distinct materials and an air layer. The wall panel is constructed of AH32 steel, while the A60 type mineral wool is utilized for its ability to facilitate stable heat transmission for a minimum of 60 min. Glass woven roving is employed for the cloth, and the cladding plate is constructed of

Table 4: Specification for each parameter

Specifications	Symbol	Unit	Value
Wall area	A	m^2	0.09
Hot side temperature	$T_{\infty 1}$	°C	950
Cold side temperature	$T_{\infty 2}$	°C	30

Table 5: Temperature calculation results for the wall surfaces from the hot side to the cold side

Type of wall	Temperature (°C)					
	T_1	T_2	T_3	T_4	T_5	T_6
W-75	844.0	839.1	113.2	113.1	—	—
W-50	850.1	850.0	569.2	564.7	108.4	108.3
W-25	724.8	724.7	714.4	200.1	200.0	—

Galvanized steel 0.5T. For further information on the parameters of these materials, please refer to Tables 3 and 4 [13,18]. Please note that the thermal conductivity values marked with "*" in Table 3 are dependent on temperature. However, as the change in thermal conductivity values is negligible when the temperature varies by tens of degrees Celsius, the calculation process will estimate the hot and cold surface temperatures to determine h_1 and h_2. For this purpose, the properties of air are being referred to Böckh and Thomas [11].

4 Result and discussion for the initial specimens

4.1 Result of theory calculation

Calculate the temperature on the surfaces of the fire-resistant wall structures W-75, W-50, and W-25 using the theoretical basis from Section 3.1. The results are displayed in Table 5.

Table 3: Material properties for each layer

Material name	Type	Thickness (L) [mm]	Density (d) [kg/m^3]	Thermal conductivity (k) [W/m K]
Wall panel	AH32	10	7,833	54–29*
Mineral wool	A60	75/50/25	130	0.04
Cloth	Glassfiber	0.5	120	0.04
Cladding plate	Galvanized steel 0.5T	0.5	7,913	13.5–26*

Note: Thermal conductivity values marked with "*" are dependent on temperature.

4.2 Result of testing

The testing procedure was as follows:

Step 1: Temperature setting of the furnace. Connect the furnace to a 220 V power source, press the start button, and then set the desired temperature to reach 950°C (temperature displayed on the screen). The furnace will be heated for approximately 2 h to reach the required temperature.

Step 2: Mount the test specimen into the furnace. Once the furnace reaches 950°C, open the furnace door and place the test specimen in the designated position inside the furnace, with the surface to be heated facing inward (the test specimen will replace the furnace door during the testing process) as shown in Figure 14.

Step 3: Measure the temperature of the outer surface of the test specimen. After the specimen has been heated, proceed to measure the temperature on the outer surface of the specimen, as presented in Figure 15. Each specimen was measured from 0 to 65 min. The measurement results are recorded in a table for further analysis (*e.g.*, Table 6 shows the measurement results for specimen W-75).

Step 4: Complete the heating process, remove the specimen, and cool. After completing the measurements, turn off the furnace, remove the test specimen from the furnace, and place it on a surface to cool down naturally. The furnace is then closed and restarted to prepare for the subsequent specimens. The temperature measurement results of the three initial test specimens are presented in Table 7 and Figure 16. The images of the test specimens before and after heating are shown in Table 8.

4.3 Result of numerical analysis

Numerical results were also conducted to enhance the reliability of experimental studies' reliability and compared them with theoretical computational results. This study utilized the ABAQUS software [19] to investigate heat transfer through the layers of all test specimens. This software suits nonlinear elastic-plastic finite element analysis and complex contact conditions for heat transfer
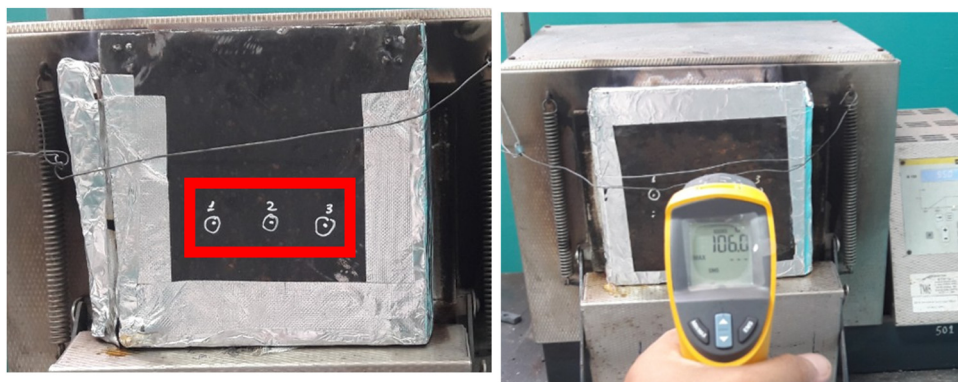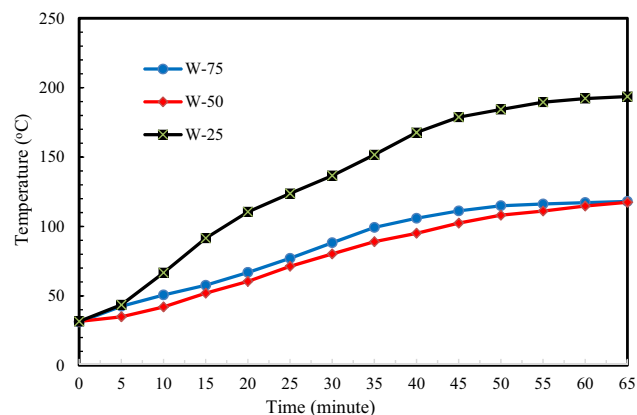

Figure 14: Setup of the specimen into the furnace.

Figure 15: Measurnments of the test specimen's temperature.

Table 6: Measured temperature values on specimen W-75

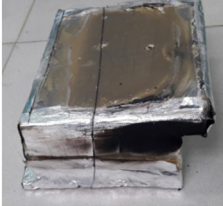| Time (min)	Measured temperature values for each location (°C)									Mean value (°C)
	Location 1			Location 2			Location 3			
	First	Second	Third	First	Second	Third	First	Second	Third	
0	31.7	31.7	31.8	32.0	32.1	32.2	29.6	29.7	29.7	31.2
5	42.8	43.1	43.1	43.3	43.5	43.6	41.0	41.0	41.2	42.5
10	51.1	51.2	51.3	51.5	51.5	52.0	49.0	49.2	49.2	50.7
15	58.1	58.2	58.2	58.6	58.5	58.6	56.0	56.1	56.3	57.6
20	67.3	67.3	67.4	67.8	67.9	67.9	65.2	65.5	65.5	66.9
25	77.2	77.3	77.6	78.1	78.2	79.0	75.1	75.2	75.6	77.0
30	88.4	88.4	88.7	89.4	89.4	89.4	86.5	86.9	87.2	88.3
35	99.7	99.8	99.8	100.1	100.3	100.4	97.8	97.8	97.8	99.3
40	106.2	106.1	106.4	106.9	106.9	106.9	104.2	104.6	104.8	105.9
45	111.4	111.5	111.8	112.2	112.2	112.3	109.7	109.7	109.9	111.2
50	115.4	115.5	115.5	115.6	116.0	116.0	113.3	113.2	113.6	114.9
55	116.6	116.7	116.7	117.1	117.1	117.3	114.5	114.7	114.9	116.2
60	117.7	117.7	117.7	118.1	118.1	118.2	115.7	115.7	115.8	117.2
65	118.1	118.1	118.2	119.1	119.4	119.7	116.4	116.4	116.8	118.0
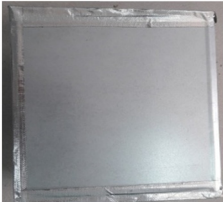
**Table 7:** Measured temperature values for the three specimens

Time (min)	Temperature of specimen (°C)		
	W-75	W-50	W-25
0	31.2	31.6	31.6
5	42.5	34.9	43.5
10	50.7	42.0	66.6
15	57.6	51.9	91.5
20	66.9	60.4	110.5
25	77.0	71.3	123.8
30	88.3	80.2	136.6
35	99.3	89.0	151.7
40	105.9	95.1	167.7
45	111.2	102.4	178.8
50	114.9	108.1	184.3
55	116.2	111.1	189.5
60	117.2	114.7	192.1
65	118.0	117.4	193.6

mechanisms. This simulation aims to predict temperature transfer through the thicknesses of thermal insulation layers. The mesh type used was shell elements (S4R). Each component's thickness was divided into five layers for integration using the Simpson rule. Sensitivity simulations were performed using several mesh sizes to establish an appropriate mesh size. The ideal mesh size was determined to be 2 × 2 mm. The chosen mesh sizes were sufficiently small to

Table 8: Results of the test specimens before and after heating

Specimen	Before heating	After heating
W-75		
W-50		
W-25		

Figure 16: Variation of temperature over time for the three specimens.
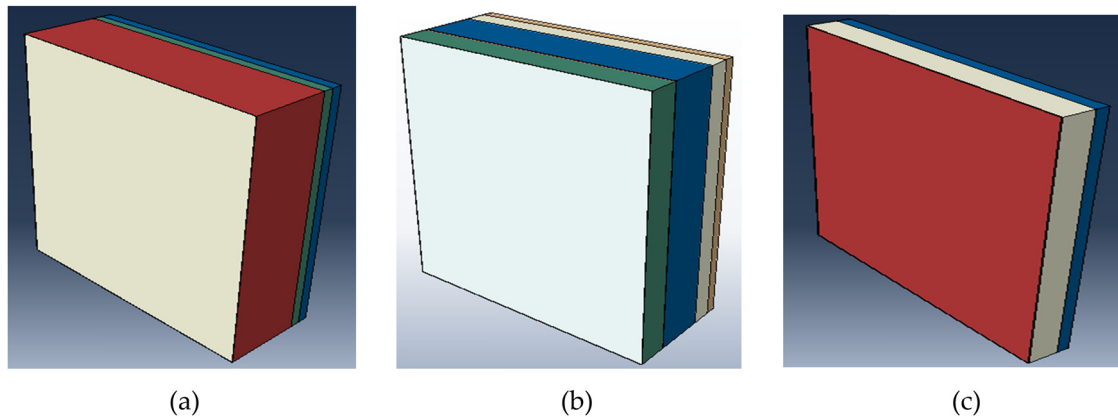
Figure 17: Modeling of multilayered insulation specimens using ABAQUS software. (a) W-75, (b) W-50, and (c) W-25.

capture heat transfer reactions precisely. Figure 17 displays the wall specimens generated by the ABAQUS program. Following the specified heat loads, a transient thermal simulation was conducted using the thermal model. The starting temperature was established at 950°C. The time length was calculated to be 3,600 s, during which the interior temperature attained dynamic equilibrium. The numerical analysis procedures followed those outlined by Chen *et al.* [20].

The steady-state temperature distribution of the multilayer insulation for a hot boundary temperature of 950°C is shown in Figure 18. The initial temperature at the boundary condition was set at 950°C. The temperature gradually decreases from the hot side to the cold side through the thickness of the insulation. It is noted that the temperature on the hot side increases to 1,099°C after 60 min. The temperature on the outermost layer of the cold side is significantly lower than the layer in contact with the hot side. Its average temperature is below 205°C. Figure 19 shows the thermal transfer distribution through the thickness of the insulation layer for samples W-75, W-50, and W-25. The detailed temperature on the outermost surface (cold side) of the specimens is presented in Table 9.

5 Discussion

The results of theoretical calculations from Table 5 show that the temperature on the outer surface (cold side) of samples W-75 and W-50 is significantly lower than the temperature requirement of the thermal insulation standard for ships [14]. Specifically, the temperatures are 113.1 and 108.3°C compared to the required 140°C. On the other hand, the outer surface temperature of specimen W-25 is much higher than the requirement at 200°C. When

examining the temperature transfer through each layer from the hot side to the cold side, it is observed that the temperature drops significantly as it passes through the mineral wool layer and the air layer (for the W-50 specimen).

The results of a test conducted on three specimens show that at the 60-min mark, the temperature measurements for specimen W-75 and W-50 were lower than the specified limit of 140°C, as presented in Figure 20. However, specimen W-25 had a significantly higher temperature of 192.1°C, which is beyond the approved regulation. Due to this, it is necessary to reevaluate practical considerations when installing this wall specimen on the ship as it may not ensure thermal insulation performance.

The temperature variation over time increases quite rapidly within the first 45 min for all three specimens. Specifically, for specimen W-75, the temperature increases approximately at a rate of 1.8°C per minute; for specimen W-50, the rate is 1.6°C per minute, and for specimen W-25, it is 3.3°C per minute. However, after 45 min, the temperature increase slows down and gradually stabilizes, with the temperature increasing at approximately 0.4°C per minute for specimen W-75, 0.8°C per minute for specimen W-50, and 0.9°C per minute for specimen W-25. From 60 min onwards, the temperature almost does not increase, which meets the stability requirement of A60-type mineral wool.

The simulation results indicate that the W-75 and W-50 specimens' outer surface temperature (cold side) is less than 140°C, which is the required temperature for the A60 fire class [17]. This finding is consistent with the theoretical and experimental computational results. However, the temperature of the W-25 specimen exceeded the required value, with a temperature value of 204.6°C, which is 46.14% higher than the required temperature.
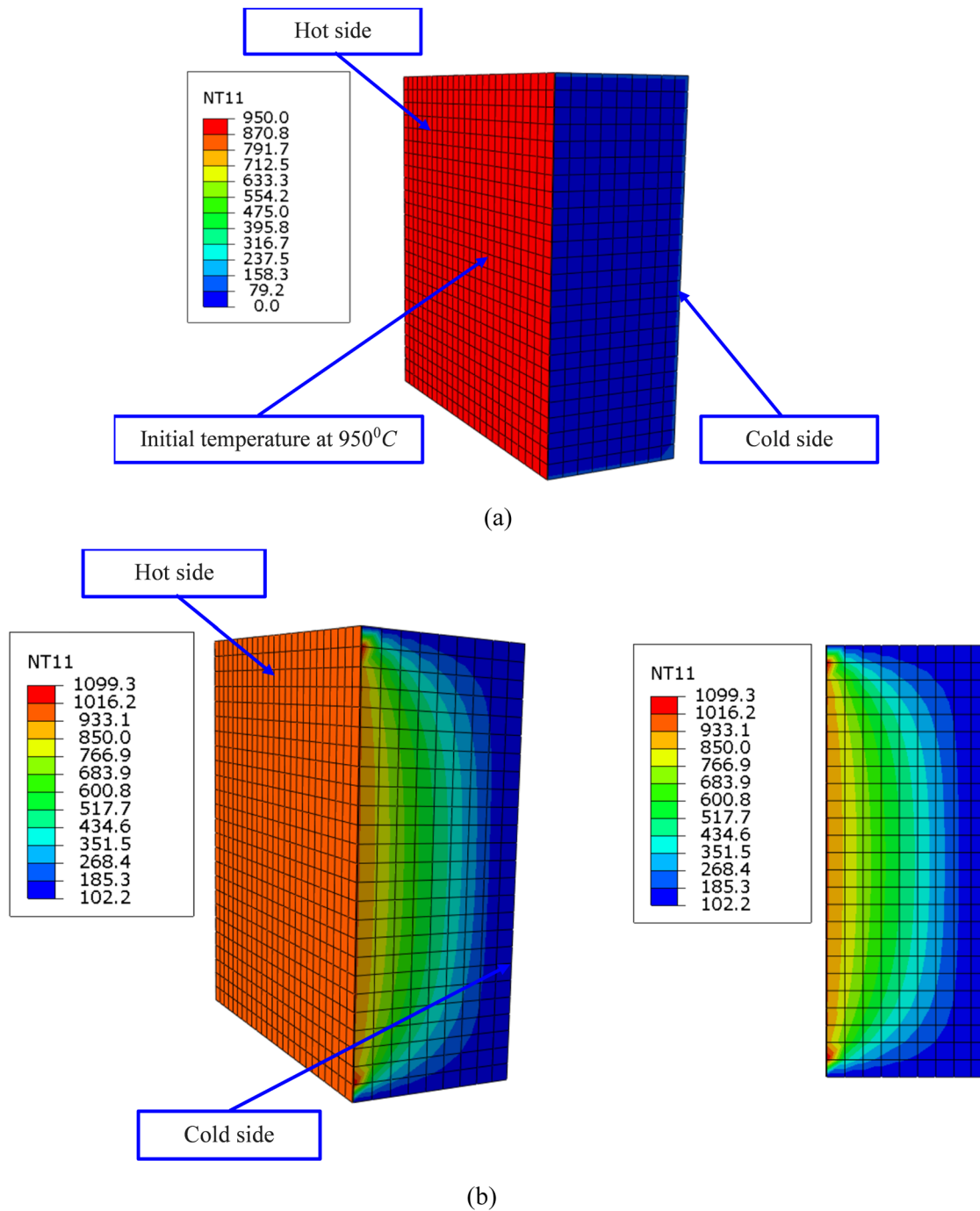
Figure 18: Temperature distribution of multi-layer insulations: (a) initial temperature at 950°C and (b) temperature through the thickness after 60 min.

Table 10 compares theoretical calculations, experimental results, and numerical analysis, indicating no significant difference in the temperatures of the panel insulation's cold side surfaces among these three methods. The modeling uncertainty factor (X_m) between theoretical and experimental results was 0.98, with a good coefficient of variation (COV) of 5.19%. Similarly, comparing numerical simulation results with experimental results, the average modeling uncertainty factor (X_m) was 0.99, while COV was 6.16%. These findings demonstrate that the numerical analysis method employed is highly accurate and reliable compared to experiments.
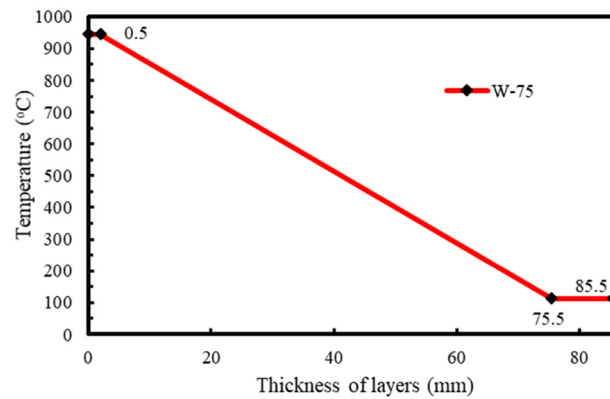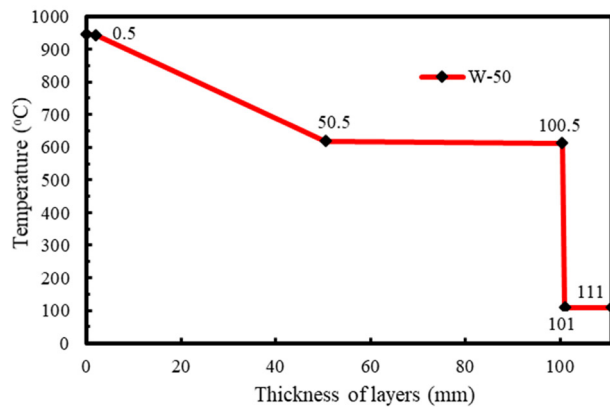
Figure 19: Distribution of temperature across the thickness of the insulation layers. (a) W-75, (b) W-50, and (c) W-25.
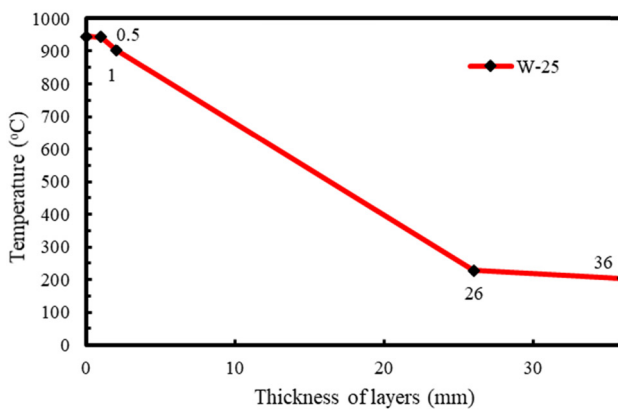
Table 9: Temperatures on cold surfaces obtained from numerical simulation results

Type of wall	Temperature at cold side area (°C)					
	T_1	T_2	T_3	T_4	T_5	T_6
W-75	945.9	945.1	113.3	113.1	—	—
W-50	945.1	944.2	618.9	612.9	109.5	109.4
W-25	945.2	944.3	903.6	228.9	204.6	—

6 Proposing strategies to optimize the thermal insulation efficiency of the wall panel

The aforementioned research results highlight the importance of thermal insulation in mineral wool and air layers. The W-25 wall type has a thin mineral wool layer (25 mm) and no air layer, which results in the outer surface temperature of the wall failing to meet the fire-resistant wall standard for ships. While increasing the thickness of the mineral wool layer to enhance thermal insulation is a possibility, it would lead to higher shipbuilding costs. To improve the thermal insulation efficiency of the wall, this study suggests adding an air layer between the wall sheet and the mineral wool layer. Specifically, for the W-50 wall type with a larger total thickness, the additional air layer is separate from the original air layer (50 mm). To evaluate the thermal insulation effectiveness of this proposed solution, each wall type is designed into three specimen types, corresponding to additional air layer thicknesses of 10, 20, and 30 mm, respectively (as shown in Figure 21). All of these wall specimens use theoretical, experimental, and numerial analysis research methods similar to the three original wall specimens.

6.1 Results for nice improved specimens

This section presents the results of predicting temperatures using theoretical, experimental, and numerical methods. In Table 11 and Figure 22, it can be seen how the temperature
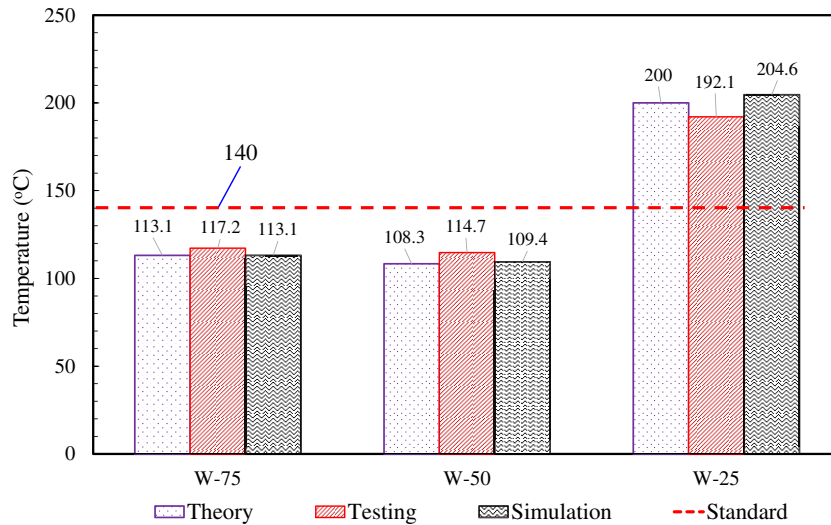
Figure 20: Comparison of the wall's outer surface temperature with the standard's requirements.

Table 10: Comparison of theoretical, experimental, and numerical temperature predictions on cold-side surfaces of wall panel insulations

Type of wall panel	Temperature (°C)			X_m (Theory/ test)	X_m (Num. analysis/ test)
	Theory	Test	Numerical analysis		
W-75	113.1	117.2	113.1	0.97	0.97
W-50	108.3	114.7	109.4	0.94	0.95
W-25	200	192.1	204.6	1.04	1.07
Mean				**0.98**	**0.99**
COV (%)				**5.19**	**6.16**

at the outermost surface of nine enhanced wall specimens was calculated using the theoretical basis from Section 3.1. Meanwhile, Table 12 and Figures 23–25 display the temperature measurement results of the nine improved test specimens. Moreover, Table 13 and Figure 26 show the temperature transmitted through the panel insulation surfaces of these nine improved test specimens. The next section will provide an in-depth discussion of these results.

6.2 Discussion for nice improved specimens

The theory, numerical, and test results demonstrate that, after improvements were made, the temperature of all specimens decreased in comparison to the initial three specimens. Notably, the improved specimens of type W-75 and W-25 showed significant temperature reductions, whereas the improved specimens of type W-50 displayed negligible reduction.

At the 60-min mark, the temperature of different specimens decreased by varying degrees. Specimen W-75-10 decreased by 19.4°C (16.5%), W-75-20 decreased by 27.7°C (23.6%), and W-75-30 decreased by 32.8°C (28.0%). Specimen W-50-10 decreased by 10.2°C (8.9%), W-50-20 decreased by 21.1°C (18.4%), and W-50-30 decreased by 26.2°C (22.8%). Similarly, specimen W-25-10 decreased by 32.4°C (16.9%), W-25-20 decreased by 63.5°C (33.1%), and W-25-30 decreased by 72.5°C (37.7%).

The temperature of specimen W-75 decreased significantly when it was improved with a 10 mm air layer. However, when the thickness of the air layer was increased to 20 and 30 mm, the temperature drop was reasonably small compared to the 10 mm specimen. Specimens W-50 and W-25 also experienced a significant temperature reduction when improved with a 10 and 20 mm air layer. However, when the thickness of the air layer was increased to 30 mm, the temperature reduction was negligible. For specimen W-25, it was only when the thickness of the air layer was increased to above 20 mm that it met the allowable temperature threshold. At the 60-min mark, the temperature of specimen W-25-20 was 128.6°C, and that of specimen W-25-30 was 119.6°C, which is below the 140°C limit.

Table 14 presents the results of temperature calculations on the cold side based on theoretical, numerical analysis, and experimental data. The average modeling uncertainty factor (X_m) between theoretical and experimental results was 0.99, with a good COV of 2.60%. Similarly, when comparing numerical analysis results with experimental results, the average X_m was 1.02, while COV was 3.44%. These results indicate that the numerical analysis method used is highly accurate and reliable compared

(a)

(b)

(c)
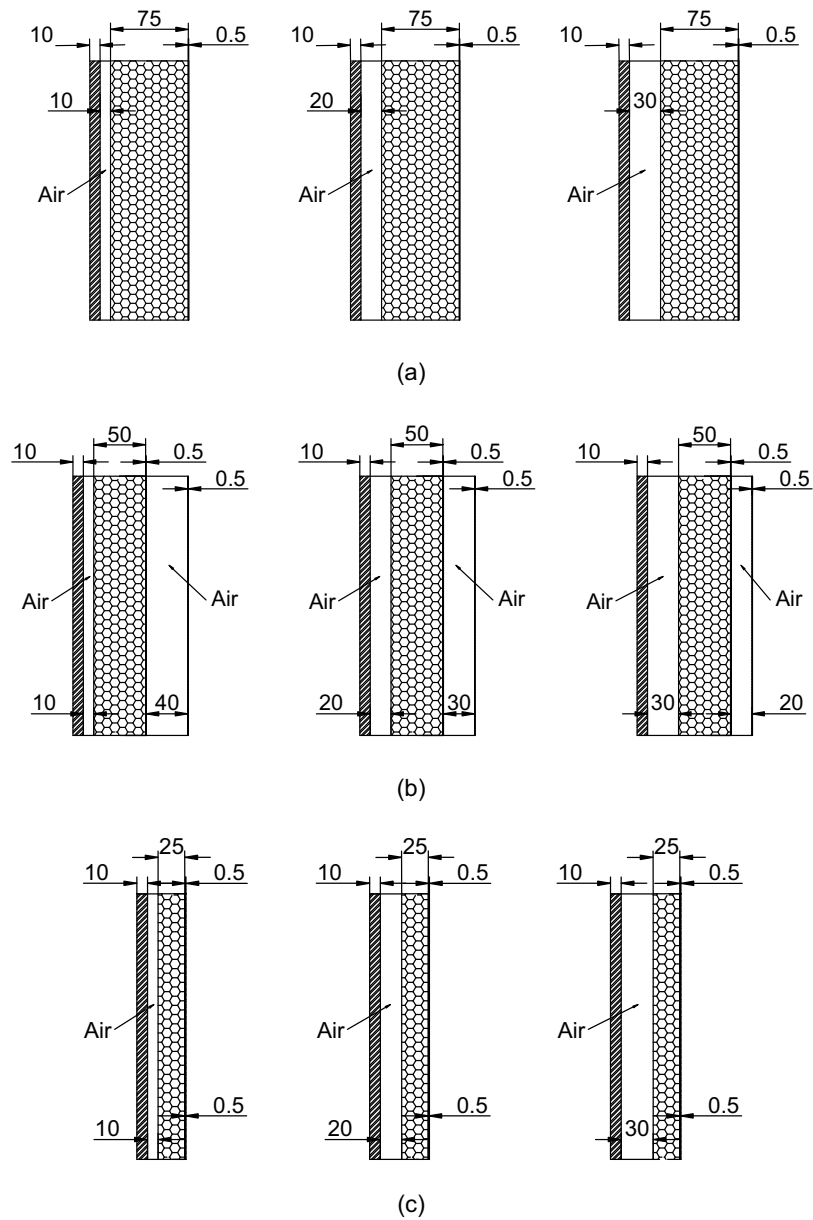
Figure 21: Improved specimens based on the three initial prototypes. (a) W-75-10, W-75-20, and W-75-30; (b) W-50-10, W-50-20, and W-50-30; and (c) W-25-10, W-25-20, and W-25-30.

Table 11: Results of temperature calculation at the surfaces of the enhanced walls

Type of wall	Temp. (°C)	Type of wall	Temp. (°C)	Type of wall	Temp. (°C)
W-75	113.1	W-50	108.3	W-25	200.0
W-75-10	101.1	W-50-10	100.9	W-25-10	156.5
W-75-20	91.5	W-50-20	93.2	W-25-20	129.1
W-75-30	83.6	W-50-30	87.0	W-25-30	114.0

to experiments. More detailed comparisons for each group of specimens are given in Figure 27.

7 Conclusion

The aim of this study was to comprehensively evaluate the thermal insulation performance of multilayered bulkhead structures used in ship engine rooms under simulated fire conditions at 950°C for 60 min. The study employed a
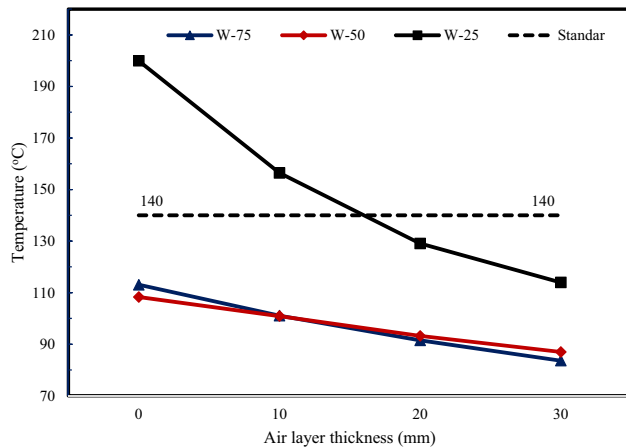
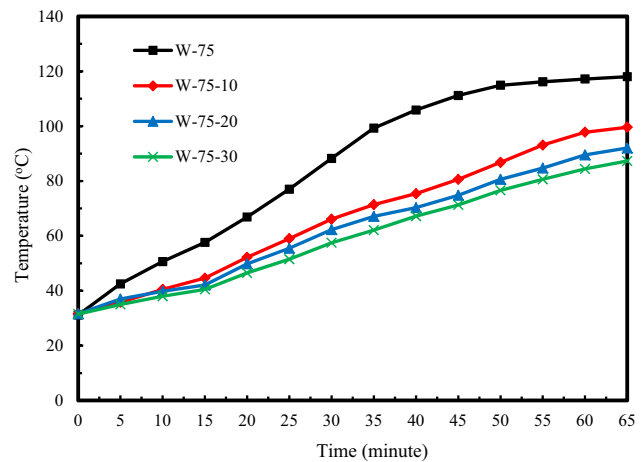**Figure 22:** Surface temperature calculations on enhanced walls.

Figure 23: Variation of temperature over time for the initial specimen and the improved specimen W-75.

combination of theoretical calculations based on heat transfer theory, experimental testing on fabricated specimens, and numerical simulations using ABAQUS software. Based on the results obtained in the present study, the following conclusions can be drawn.

First, the results obtained from testing the three original bulkhead specimens (W-75, W-50, and W-25) with different mineral wool thicknesses of 75, 50, and 25 mm, respectively, revealed that only W-75 and W-50 met the regulatory requirement of maintaining an outer surface temperature below 140°C. Specifically, the outer surface temperatures were 117.2°C for W-75 and 114.7°C for W-50 from experiments. However, the W-25 specimen exceeded this limit with an outer temperature of 192.1°C, highlighting the need for design improvements.

Second, to enhance the thermal insulation capabilities of the underperforming W-25 bulkhead type, a novel
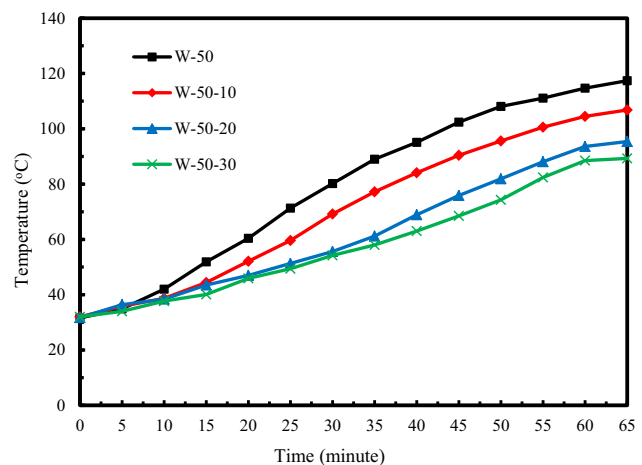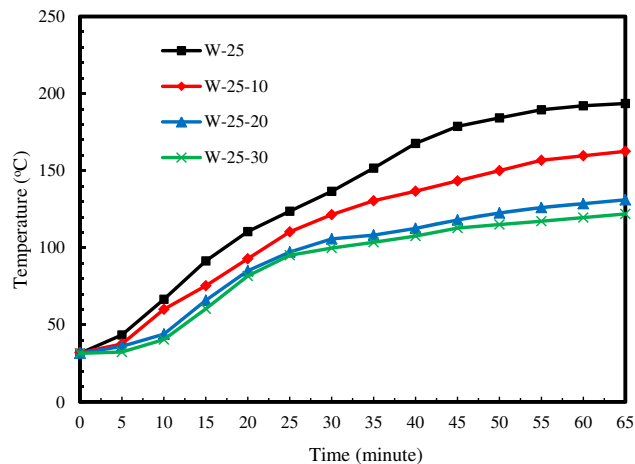

Figure 24: Variation of temperature over time for the initial specimen and improved specimen W-50.

Table 12: Measured temperature values for nine improved test specimens

Time (min)	Specimen's temperature (°C)								
	W-75-10	W-75-20	W-75-30	W-50-10	W-50-20	W-50-30	W-25-10	W-25-20	W-25-30
0	31.6	31.6	31.5	32.0	31.7	32.0	32.0	31.6	31.6
5	35.8	37.0	35.0	35.8	36.4	34.0	37.6	36.1	32.4
10	40.5	39.8	38.0	38.7	38.4	37.7	60.1	44.0	40.5
15	44.6	42.1	40.5	44.4	43.5	40.1	75.4	65.9	60.4
20	52.2	49.8	46.5	52.1	47.0	45.9	92.9	85.1	81.7
25	59.0	55.5	51.5	59.6	51.3	49.4	110.4	97.2	95.2
30	66.1	62.3	57.5	69.2	55.6	54.2	121.5	105.8	99.8
35	71.4	67.1	62.1	77.2	61.2	58.0	130.5	108.2	103.6
40	75.4	70.3	67.2	84.1	68.9	63.0	136.7	112.6	107.6
45	80.6	74.8	71.3	90.4	75.9	68.5	143.4	118.1	112.8
50	86.8	80.6	76.6	95.6	81.9	74.3	150.1	122.6	115.1
55	93.1	84.7	80.6	100.6	88.1	82.4	156.8	126.1	117.2
60	97.8	89.5	84.4	104.5	93.6	88.5	159.7	128.6	119.6
65	99.6	92.0	87.3	106.8	95.4	89.3	162.6	131.1	122.0

Figure 25: Variation of temperature over time for the initial specimen and improved specimen W-25.
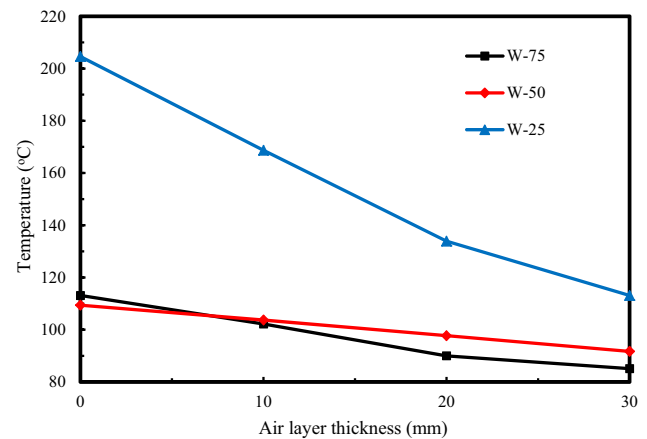
Figure 26: Temperature at cold side surface for three original and nine improved specimens.

strategy was implemented by introducing air gaps of 10, 20, and 30 mm thicknesses between the wall panel and the mineral wool layer. This resulted in nine improved specimen configurations. Incorporating these air gaps led to significant reductions in the outer surface temperatures compared to their original specimens. Among the improved specimens, those derived from the W-25 type exhibited the most substantial temperature decreases. Notably, the W-25-20 specimen achieved an outer surface temperature of 128.6°C, while the W-25-30 specimen reached 119.6°C after 60 min of fire exposure, successfully meeting the required temperature limit below 140°C.

Third, to validate the reliability of the findings, the study compared the estimated heat transfer results obtained through theoretical calculations and numerical simulations with the experimental data. The high degree of agreement between these three methodologies was evidenced by a low average modeling uncertainty factor (X_m) of 0.99 between

theory and experiments (COV with 2.60%) and 1.02 between numerical analyses and experiments (COV with 3.44%).

Fourth, this research has demonstrated the efficacy of incorporating air gaps within the multilayered insulation structure to enhance the thermal insulation performance of ship engine room bulkheads. Specifically, for the critical W-25 bulkhead type, the inclusion of an air gap with a thickness of at least 20 mm proved crucial in ensuring compliance with the stipulated temperature requirement of below 140°C.

Finally, while this study's findings are promising, further investigations are recommended to explore the application of this design approach incorporating air gaps to different wall panel types, vessels, and insulation materials. This would broaden the scope and practical implications of these research endeavors in improving the fire safety and thermal management of marine vessels and offshore structures.

Table 13: Temperature values transmitted through the panel insulation surfaces for nine improved test specimens

Temp. through each thickness	Temperature values (°C)								
	W-75-10	**W-75-20**	**W-75-30**	**W-50-10**	**W-50-20**	**W-50-30**	**W-25-10**	**W-25-20**	**W-25-30**
T_1	945.8	945.8	945.8	945.1	945.1	945.1	945.2	945.2	945.2
T_2	939.3	939.8	939.2	945.0	945.0	944.9	944.9	944.9	944.9
T_3	218.3	301.6	367.6	703.7	780.6	847.6	934.3	937.0	937.6
T_4	102.3	93.1	85.2	698.0	775.1	842.5	484.6	603.3	673.6
T_5	102.2	93,0	85.1	219.1	323.6	421.0	168.9	134.0	113.2
T_6	—	—	—	103.8	97.8	91.8	168.7	133.9	113.1
T_7	—	—	—	103.7	97.7	91.7	—	—	—

Table 14: Comparison of theoretical, experimental, and numerical temperature predictions on cold-side surfaces of wall panel insulations for nice improved specimens

Type of wall	Temperature (°C)			X_m (Theory/test)	X_m (Num. analysis/test)
	Theory	Test	Numerical analysis		
W-75-10	101.1	97.8	102.2	1.03	1.04
W-75-20	91.5	89.5	90.0	1.02	1.01
W-75-30	83.6	84.4	85.1	0.99	1.01
W-50-10	100.9	104.5	103.7	0.97	0.99
W-50-20	93.2	93.6	97.7	1.00	1.04
W-50-30	87.0	88.5	91.7	0.98	1.04
W-25-10	156.5	159.7	168.7	0.98	1.06
W-25-20	129.4	128.6	133.9	1.01	1.04
W-25-30	114.0	119.6	113.1	0.95	0.95
Mean				**0.99**	**1.02**
COV (%)				**2.60**	**3.44**
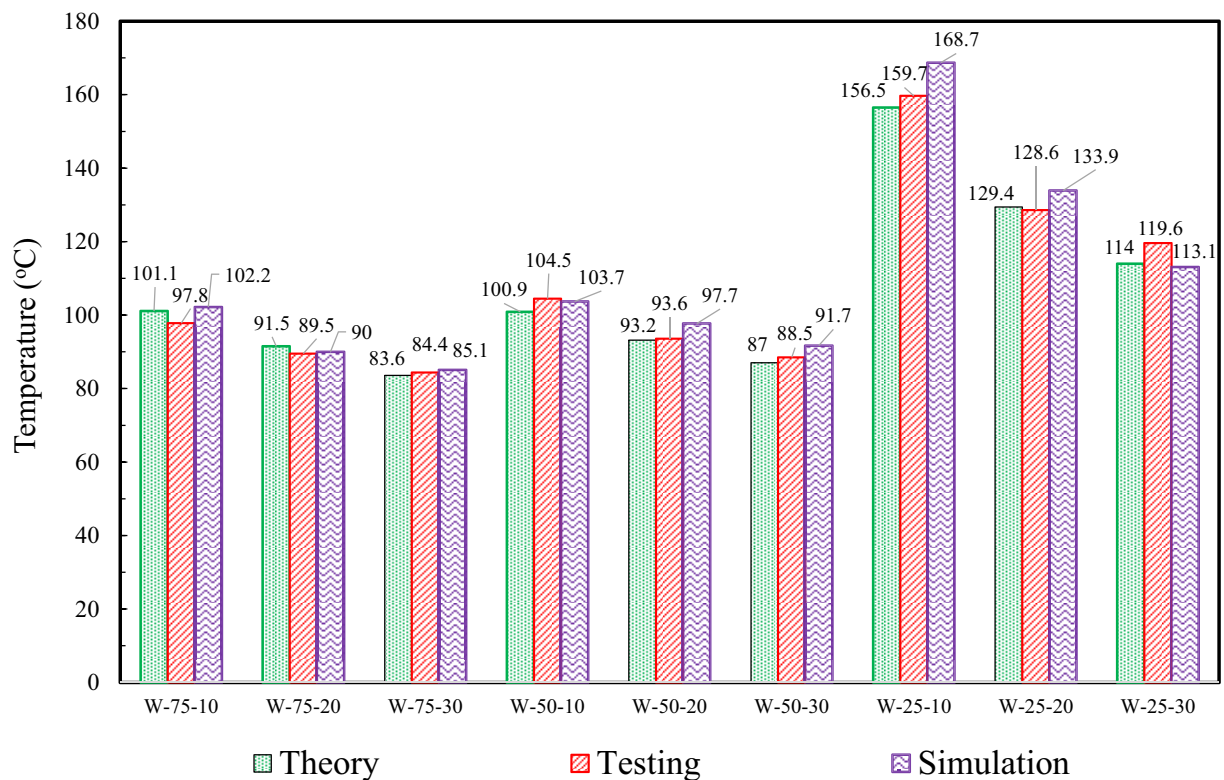
Figure 27: Comparing theoretical, experimental, and numerical temperature predictions on the cold-side surfaces of wall panel insulations for nine improved specimens.

Author contributions: Thanh-Nhut Pham: conceptualization, project administration, writing – original draft, and writing – review and editing. Quoc Tien Le: experiments and numerical analysis. Quang Thang Do: conceptualization, writing – original draft, and writing – review and editing, and developed the numerical method and validation. All authors have accepted responsibility for the entire content of this manuscript and approved its submission.

References

[1] Standard practice. Standard practice 2011 Wall/Ceiling/Lining in accom - 82,000 DWT class bulk carrier; 2011. p. 1–200.

[2] Morgan. Marine and offshore fire divisions bulkhead, deck and floor systems. Morgan Thermal Ceramics; 2013. p. 1–48.

[3] Isover SG. Insulation guide marine & offshore - For safe, comfortable and sustainable ships. Marine manual. La Défense Cedex, France: Isover SG; 2011. p. 1–48.

[4] Keith RM. Plant engineering handbook. Boston: Butterworth-Heinemann; 2001. p. 1–1189.

[5] Richard T, Bynum JR. Insulation handbook. Washington DC, USA: The McGraw-Hill Companies; 2001. p. 1792–1808.

[6] Mahdi QA, Mhmood IA, Mashhour MA. Thermal fatigue analysis of different nano coating thickness by air plasma spraying in diesel engine thermal barrier coating. Curved Layer Struct. 2022;9:365–81.

[7] Dimitri R, Rinaldi M, Tornabene F, Micelli F. Numerical study of the FRP-concrete bond behavior under thermal variations. Curved Layer Struct. 2023;10:20220193.

[8] Mahajan VM, Sharma A. Evaluation of static responses for layered composite arches. Curved Layer Struct. 2023;10:20220185.

[9] Mohammed AJ, Kadhom HK. Flutter investigation and deep learning prediction of FG composite wing reinforced with carbon nanotube. Curved Layer Struct. 2024;11:20220218.

[10] Tuswan T, Zubaydi A, Piscesa B, Ismail A, Ariesta RC, Prabowo AR. A numerical evaluation on nonlinear dynamic response of sandwich plates with partially rectangular skin/core debonding. Curved Layer Struct. 2022;9:25–39.

[11] Böckh PV, Thomas W. Heat transfer - Basics and practice. Heidelberg Dordrecht London New York: Springer; 2012. p. 1–276.

[12] Kevin GH. Heat transfer - Introduction. Johannesburg, Gauteng, South Africa: University of the Witwatersrand; 2021. p. 1–140.

[13] John HL. A heat transfer textbook. 3rd edn. Cambridge, Massachusetts, USA: Phlogiston Press; 2008. p. 1–739.

[14] Yizhou J, Duanfeng H, Ziwei Z. Research of flammability of fireproof materials in ship safety. Int conference and Nanomaterials. Barcelona, Spain; 2017. p. 1–7.

[15] Pierre M, David T. Characterization of composite thermal insulation for marine riser structures. ASME - Pressure Vessels and Piping Conference. Boston, Massachusetts, USA; 2015. p. 1–6.

[16] Yunus AC, Afshin JG. Heat and mass transfer: Fundamentals and applications. 6th edn. New York, USA: Mc Graw Hill Education; 2020. p. 1–992.

[17] National Technical Regulations on Classification and Construction of Steel-Hulled Ships - Part 5: Fire Prevention, Detection, and Suppression. QCVN 21:2015/BGTVT. BGTVT; 2015.

[18] Maurice S. Material requirements: Piping materials. Surf Prod Oper. 2016;3:159–92.

[19] ABAQUS User's Manual Version 6.13; 2013.

[20] Chen MJ, Zhang P, Li Q. Design and heat transfer analysis of a compound multi-layer insulations for use in high temperature cylinder thermal protection systems. Sci China Technol Sci. 2018 Jul;61(7):994–1002.